Received: 5 July 2024 | Revised: 1 October 2024 | Accepted: 14 October 2024

DOI: 10.1002/mma.10579

RESEARCH ARTICLE

WILEY

Analytical approach in designing PID controller for complex fractional order transfer function

Uğur Demiroğlu[1] | **Bilal Şenol**[2] | **Radek Matušů**[3]

[1]Software Engineering Department, Faculty of Engineering, Architecture and Design, Kahramanmaraş İstiklal University, Kahramanmaraş, Türkiye

[2]Software Engineering Department, Faculty of Engineering, Aksaray University, Aksaray, Türkiye

[3]Centre for Security, Information and Advanced Technologies (CEBIA–Tech), Faculty of Applied Informatics, Tomas Bata University in Zlín, Zlin, Czech Republic

Correspondence
Bilal Şenol, Software Engineering Department, Faculty of Engineering, Aksaray University, Aksaray, Türkiye.
Email: bilal.senol@aksaray.edu.tr

The study focuses on the fractional complex order plant model, which has gained popularity in applied mathematics, physics, and control systems. A significant contribution of this research lies in discussing the physical phenomena associated with complex plant models and their impact on system stability and robustness. The main purpose of the method presented in this paper is to tune the controller parameters to ensure the stability and robustness of the system. There are methods presented in the literature for this purpose. One of these methods is to keep the phase curve in the system frequency response flat within a certain range. However, this process is based on equating the derivative of the phase value to zero at a certain frequency and adds great mathematical complexity to the calculations. In this study, reliable analytical formulas are presented for the same purpose using a graphical approach. Since the fractional complex order plant model represents the most general mathematical form, it enables easy creation of other plant models, including integer order and fractional order plant. The reason why this plant is chosen is that this structure can be named as the universal plant, which all other structures can be built by making little variations. For instance, a transfer function having integer, real and/or complex number coefficients and/or orders can be obtained by proper determination of the parameters of the universal plant. A time delay can also be added towards researcher's desire. The main inspiration comes from studying on an inclusive plant. The method in this paper intends to tune the well-known classical Proportional Integral Derivative controller. Thus, effectiveness of the integer order controller on various plants will be shown. This approach provides analytical calculation equations for the physical modifications of plants with integer, fractional, and/or complex coefficients and/or orders. The effectiveness of the method is demonstrated visually with different examples that include these different possible situations. The results observed in the changes of the parameters in the transfer functions were also examined. Thus, pros and cons of the variations of integer, fractional, and complex numbers on system parameters have been shown.

KEYWORDS

analytical method, controller design, fractional complex order, fractional order, integer order, proportional integral derivative

MSC CLASSIFICATION

34A25, 93C83, 11Y16, 26A33

1 | INTRODUCTION

In the context of actual industrial processes, ensuring reliable and effective operation of sophisticated control systems places a significant burden on controllers [1]. Proportional-Integral-Derivative (PID) controllers find widespread use in modern industrial applications [2–4] particularly in process control [5]. However, PID controllers lack long-term memory effects, which are present in other complex systems associated with non-local dynamics. To enhance accuracy in modeling, fractional calculus—allowing integration and differentiation of arbitrary orders—becomes relevant [6, 7]. While integer-order calculus forms the basis for common PID models used in control applications, it lacks the non-locality feature associated with fractional derivatives [8, 9]. The well-known auto-tuning technique developed by Ziegler and Nichols [10] finds applications in diverse research areas, including thermal diffusion, chaotic systems, viscoelasticity, signal processing, mechatronic systems, and neural networks [11–17]. This technique plays a crucial role in providing detailed descriptions of physical processes in the real world [18]. For example, fractional-order derivatives have been successfully employed in controlling hydraulic servo systems with significant mechanical inertia and historical dependence. Furthermore, fractional calculus plays a pivotal role in system modeling and controller design studies [19–22].

The study investigates the physical phenomenon of solutions generated using the Fractional Complex Order Plant (FCOP) model and the classical PID controller structure. It would be useful to give brief information about the controller structure for the beginning. The PID controller, also known as the three-term controller, is a widely used feedback control mechanism in industrial systems and various other applications [23]. Its purpose is to continuously modulate control signals to maintain a desired setpoint by minimizing the error between the setpoint and the measured process variable. The three terms in the PID algorithm can be summarized. The proportional (P) term is proportional to the current error between the setpoint and process variable. It adjusts the control output based on the gain factor K_p. For instance, if the error is large, the control output will be proportionately adjusted to reduce the error. However, using proportional control alone can result in a steady-state offset between SP and process variable. The integral (I) term accounts for past errors and integrates them over time. It aims to eliminate any residual error by adding a control effect based on the cumulative value of historical errors. The integral term helps achieve precise control even in steady-state conditions. The derivative (D) term considers the rate of change of the error. It helps prevent overshoot and oscillations by adjusting the control output based on how quickly the error is changing. The D term provides stability and responsiveness. The PID controller combines these three terms to calculate the control output, adjusting a control variable (e.g., opening a valve) to minimize the error over time. Since tuning these three parameters conveniently is significant, mathematical methods play an important role in this issue.

In control theory, a plant refers to the combination of a process and an actuator. The plant is often described using a transfer function, typically in the s-domain. This transfer function represents the relationship between an input signal and the output signal of a system without feedback. It's commonly determined by the physical properties of the system. For real-world processes, determining the transfer function of the plant involves using system identification methods with experimental data. These transfer functions are mostly described by integer-order polynomials in the numerator and denominator. Integer-order representation is generally preferred for convenience on modeling real-world processes. However, real-world processes can be expressed more accurately with fractional order transfer functions [24, 25]. This concept has gained increasing attention in recent years despite its complicated structure [26].

This paper deals with an even more complicated structure of transfer function, which has polynomials having orders of complex numbers. This new structure covers all types of transfer functions including fractional- and integer-order ones with time delay. The transfer function is detailly explained in following sections. Let us investigate the existing studies about the subject. Fractional-order approximations are mostly derived numerically; thus, numerical simulation of the fractional-order control system is studied in [27, 28]. The PID controller is also thought to have fractional orders

in the literature. Different papers explain various fractional-order PID (FOPID) tuning procedures in both frequency and time domain design methodologies [29–31]. The design approach for fine-tuning a fractional complex-order PI (FCOPI) controller was the main emphasis of Shahiri et al. [32]. An optimization-based method for fine-tuning actual and sophisticated FOPI controllers was presented by Moghadam et al. [33]. In their work, Muresan et al. [34] investigated a simple method based on vector representation of fractional-order controllers. The fractional complex-order controller (FCOC) was investigated by Guefrachi et al. [35], and the fractional-order controller (FOC) was explored by Hanif et al. [36] using a genetic algorithm. Important studies on complex-order fractional diffusion [37] and complex-order capacitive impedance realization [38] have just been released. The tuning of fractional complex-order DC motor in the frequency domain can be found in [39]. These studies demonstrate the significant increase in attendance at the FCOP during the past few years. Researchers are now investigating the potential applications of fractional complex order in control theory and system modeling as can be seen in the studies in [40–43]. In addition, the preliminaries of this study were presented for the proportional-derivative controller in [44].

This study explores the use of the FCOP model and the PID controller structure, which are gaining popularity in applied mathematics, physics, and control systems. The research investigates analytical solutions and the associated physical phenomena. A complex system with an underexplored controller structure is considered. The study examines stability and robustness outcomes for various parameter values, supported by simulations and graphics. Additionally, the impact of the complex coefficient's real and imaginary components is analyzed during the design process.

It would be beneficial to provide an overview of this study's key points and its contribution to the literature. The primary goal of this research is to design a controller that ensures the stability and robustness of a model. The model used is a complex fractional-order model, which is relatively new in the field of control. This model allows for the derivation of both classical integer- and fractional-order models and can incorporate time delays. Consequently, a comprehensive transfer function encompassing various structures is proposed.

The study focuses on the widely used PID controller design within the control domain to ensure the stability and robustness of the model described by the comprehensive transfer function. The method involves adjusting the system's frequency characteristics to meet the researcher's specifications. Systems are typically represented in the frequency domain by gain and phase values. The main objective in designing the controller is to achieve the desired gain and phase characteristics, ensuring stability and robustness. For a better understanding of the presented method, a summary illustration is given in Figure 1.

According to Figure 1, brief explanation of the method can be written. The universal plant is defined first. It can be a plant having integer, fractional, or complex coefficients or orders. The frequency domain properties desired to be satisfied are determined next. Then, these properties are combined with the proposed formulas, and the controller to achieve these properties is obtained. Let us investigate the figure in a closer look. The frequency properties are the gain crossover frequency (ω_{gc}), the phase crossover frequency (ω_{pc}), and the phase margin (PM). Related studies in the literature proved that the magnitude (gain) and phase curves have effect on the system behavior. For example, the phase curve between ω_{gc} and ω_{pc} (the curve through x) is flattened to increase system robustness [44]. Graphically, this is done by extending the distance between these crossover frequencies. Additionally, the PM is tuned by changing the

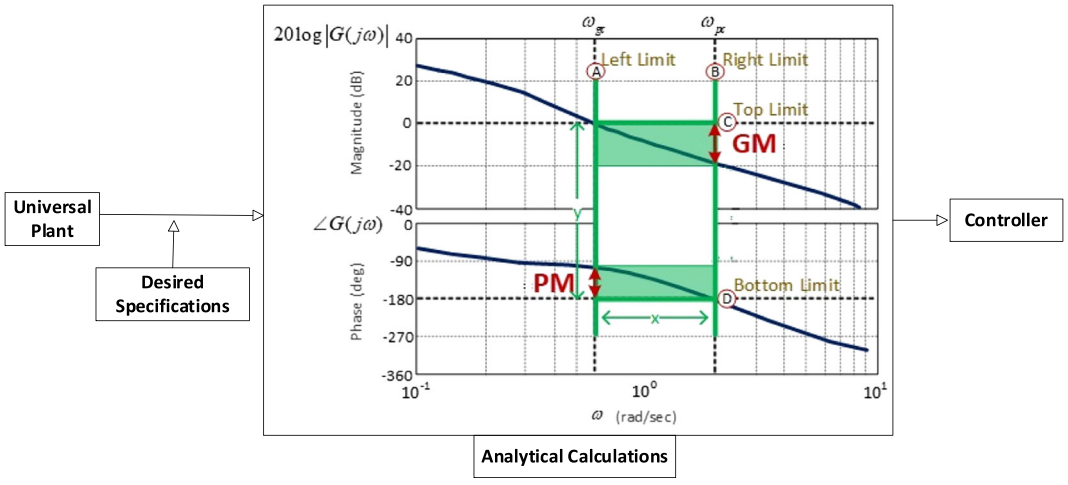

FIGURE 1 Brief illustration of the presented method. [Colour figure can be viewed at wileyonlinelibrary.com]

vertical line y. The proposed formulations to calculate the controller are built on this inspiration. Detailed information is provided in the advancing sections of the paper.

The method's reliance on analytical calculations enhances its reliability. This approach is significant for the literature, as studies on complex fractional-order systems, which are more intricate than classical systems, remain limited. Therefore, the findings of this research are expected to contribute significantly to the study of complex fractional-order models. For convenience, the common abbreviations used throughout the paper are listed in Table 1.

The following are the important points of the study. Section 2 discusses the closed loop properties of the system. In Section 3, design of the universal plant is studied and in Section 4, design of the PID controller is given. The design procedure of the auto-tuning system is discussed in Section 5. Three application examples are offered in Section 6 along with the benefits of calculating equations. The results of the investigation into the physical interpretations of the obtained solutions are addressed in Section 7 and the study's key findings are presented in Section 8.

2 | PROPERTIES OF THE SYSTEM

Figure 2 shows the representation of a closed loop control system. As known, real processes can be modeled using differential equations. For convenience, the differential equations are transformed to the s domain by the Laplace transform [45]. Here, $P(s)$ and $C(s)$ are the Laplace transform output of the differential equation models of the plant and controller respectively. R(s) is the Laplace sign of the input signal, and $Y(s)$ is the signal for the output of the system. It can be said that the system's closed-loop transfer function is closely related to its open-loop transfer function [46, 47]. $D(s)$ is the disturbance signal introduced at the end of this section, and $E(s)$ is the error signal obtained by subtracting output from the input.

Open loop ($G[s]$) representation of the system is

$$G(s)=\frac{Y(s)}{R(s)}=P(s)C(s). \tag{1}$$

Open loop transfer function is obtained by excluding the disturbance signal and the feedback loop shown with the arrow connecting the system output to the system input. Therefore, the transfer function of the system is obtained by direct multiplication of the plant and the controller [45]. Similarly, the closed loop representation ($T[s]$) is

$$T(s)=\frac{Y(s)}{R(s)}=\frac{P(s)C(s)}{1+P(s)C(s)}=\frac{G(s)}{1+G(s)}. \tag{2}$$

Here, the closed loop transfer function can be obtained easily by the following procedure. The error signal $E(s)$ is $E(s)=R(s)-Y(s)$. There is a feedback loop here; thus, the equation $Y(s)=G(s)[R(s)-Y(s)]$ is valid. This yields to $Y(s)=\frac{G(s)}{1+G(s)}R(s)$, and then, the closed loop transfer function is obtained. In order to clearly understand the analytical

TABLE 1 List of the common abbreviations used in the paper.

Abbreviation	Explanation
FCOP	Fractional complex order plant
PID	Proportional-integral-derivative
FOPID	Fractional order proportional-integral-derivative

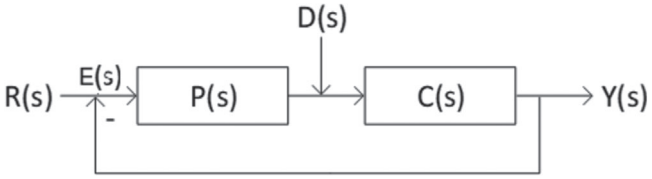

FIGURE 2 The closed loop control system.

design approach in this paper, some background information should be useful. The Bode diagram is a type of graph used in system analysis that combines the system's gain and PM graphs. This combination in a single image is highly convenient. Bode diagrams are used to analyze open-loop systems. The gain margin (GM), the first component of the system, indicates how much the open-loop system's gain can be increased while maintaining stability. The PM, the second component, shows how much the open-loop system's phase can be increased to ensure system stability [48, 49].

The gain crossover frequency is ω_{gc}, and the phase crossover frequency is ω_{pc} in the Bode diagram. The gain crossover frequency is the frequency at which the curve on the gain graph cuts 0 dB line, and the phase crossover frequency is the frequency value where the phase curve cuts the -180° line. The GM is the difference between the current gain value with the 0 dB line at ω_{pc}. The PM is the difference between the current phase value with the -180° line at ω_{gc}. GM shows the amount by which the gain can be increased to ensure system stability, while PM indicates the extent to which the phase can be adjusted while maintaining system stability.

The following equations provide the phase and gain of the system at the gain crossover frequency.

$$\angle \mathrm{G(s)}|_{\mathrm{s=j}\omega_{gc}} = PM - \pi, \tag{3}$$

$$|G(s)||_{s=j\omega_{gc}} = 1. \tag{4}$$

Similarly, the following equations provide the phase and gain of the system at the phase crossover frequency.

$$\angle \mathrm{G(s)}|_{\mathrm{s=j}\omega_{pc}} = -\pi, \tag{5}$$

$$|G(s)||_{s=j\omega_{pc}} = 10^{GM/20}. \tag{6}$$

In summary, above equations indicate the properties of an ideal system. Phase of the system at ω_{gc} is $PM - \pi$, and gain of the system is 1. At ω_{pc}, phase of the system is $-\pi$, and the gain is $10^{GM/20}$. It can be said that the gain and phase crossover frequencies of the Bode diagram are closely related to the system's stability and robustness over a wide range.

Systems can be due to unexpected disturbance signals. In order the system to be robust against these effects, the design procedure gets more challenging. The current error of a system increases when it encounters unexpected load disturbance signals, which are defined as unwanted external input signals to the system. Designing a stable system is a crucial step in system design. However, in stable systems, it is even more critical to avoid or fully eliminate system failures that may arise from such unexpected load disturbance signals. $D(s)$ in Figure 1 denotes the load disturbance signal $D(s)$ [50–53]. The disturbance is usually represented with a unit step signal in the literature [44]. The following equation gives the partial function representation of the load disturbance signal.

$$u(t-a) = \begin{cases} 1 & t \geq a \\ 0 & t < a \end{cases}. \tag{7}$$

The charge disturbance signal's input Laplace sign is obtained by converting $d(t) = u(t-a)$.

$$D(s) = \frac{1}{s}\mathrm{e}^{-as}. \tag{8}$$

After the preliminaries, design of the FCOP can be done.

3 | DESIGN OF THE UNIVERSAL PLANT

The following equation represents the most general plant transfer function that can be encountered, featuring integer, fractional, and complex number coefficients, as well as exponential, time-delayed, or non-delayed extra gain coefficients [44].

$$P(s) = K\frac{\sum_{i=0}^{m}(ae_i + jao_i)s^{(\alpha e_i + j\alpha o_i)}}{\sum_{k=0}^{n}(be_k + jbo_k)s^{(\beta e_k + j\beta o_k)}}e^{-Ls}. \tag{9}$$

The gain is denoted by K, and the time delay is L. To simplify the presentation, certain notations are introduced. e stands for even, and o denotes odd. Thus, the even parts of the coefficients and orders of the numerator are denoted by ae_i and αe_i, respectively. The odd parts are represented by ao_i and αo_i in similar. For the denominator, be_k and βe_k represent the even parts of the coefficients and orders, respectively. Finally, bo_k and βo_k are the odd parts of the coefficients and orders. The e in e^{-Ls} stands for the exponent operator.

The following gives the plant frequency response of the above transfer function.

$$P(j\omega) = K\frac{\sum_{i=0}^{m}(j\omega)^{\alpha e_i + j\alpha o_i}(ae_i + jao_i)}{\sum_{k=0}^{n}(j\omega)^{\beta e_k + j\beta o_k}(be_k + jbo_k)}e^{-L(j\omega)}. \tag{10}$$

With the use of Euler's equation, a complex number in the numerator of the plant frequency response can be represented simply as shown in Equation (11), by transforming from exponential form to trigonometric form and vice versa.

$$(j\omega)^{\alpha e_i + j\alpha o_i} = e^{-\frac{\pi\alpha o_i}{2}}\omega^{\alpha e_i}\left(\cos\left(\frac{\pi\alpha e_i}{2} + \log(\omega)\alpha o_i\right) + j\,\sin\left(\frac{\pi\alpha e_i}{2} + \log(\omega)\alpha o_i\right)\right). \tag{11}$$

Similarly, Equation (12) stands for the transformation of the complex order of the denominator polynomial.

$$(j\omega)^{\beta e_k + j\beta o_k} = \mathrm{e}^{-\frac{\pi\beta o_k}{2}}\omega^{\beta e_k}\left(\cos\left(\frac{\pi\beta e_k}{2} + \log(\omega)\beta o_k\right) + j\,\sin\left(\frac{\pi\beta e_k}{2} + \log(\omega)\beta o_k\right)\right). \tag{12}$$

Then, the plant frequency response can be re-expressed as Equation (13) by changing the formulas in Equations (11) and (12) to exponential form.

$$P(j\omega) = K\frac{\sum_{i=0}^{m}\mathrm{e}^{-\frac{\pi\alpha o_i}{2}}\omega^{\alpha e_i}\mathrm{e}^{j\left(\frac{\pi\alpha e_i}{2} + \log(\omega)\alpha o_i\right)}(ae_i + jao_i)}{\sum_{k=0}^{n}\mathrm{e}^{-\frac{\pi\beta o_k}{2}}\omega^{\beta e_k}\mathrm{e}^{j\left(\frac{\pi\beta e_k}{2} + \log(\omega)\beta o_k\right)}(be_k + jbo_k)}\mathrm{e}^{-jL\omega}. \tag{13}$$

Equation (14) re-expresses the plant frequency response described in Equation (13) in a broad form.

$$P(j\omega) = K\frac{(ne + jno)}{(de + jdo)}\mathrm{e}^{-jL\omega}. \tag{14}$$

In Equations (15) and (16), the ne even part and no odd part of the numerator composing the plant's frequency response are given, respectively.

$$ne = \sum_{i=0}^{m}\mathrm{e}^{-\frac{\pi\alpha o_i}{2}}\omega^{\alpha e_i}\left(\cos\left(\frac{\pi\alpha e_i}{2} + \log(\omega)\alpha o_i\right)ae_i - \sin\left(\frac{\pi\alpha e_i}{2} + \log(\omega)\alpha o_i\right)ao_i\right), \tag{15}$$

$$no = \sum_{i=0}^{m}\mathrm{e}^{-\frac{\pi\alpha o_i}{2}}\omega^{\alpha e_i}\left(\sin\left(\frac{\pi\alpha e_i}{2} + \log(\omega)\alpha o_i\right)ae_i + \cos\left(\frac{\pi\alpha e_i}{2} + \log(\omega)\alpha o_i\right)ao_i\right). \tag{16}$$

In Equations (17)–(18), the de even part and do odd part of the denominator composing the plant's frequency response are given, respectively.

$$de = \sum_{k=0}^{n}\mathrm{e}^{-\frac{\pi\beta o_k}{2}}\omega^{\beta e_k}\left(\cos\left(\frac{\pi\beta e_k}{2} + \log(\omega)\beta o_k\right)be_k - \sin\left(\frac{\pi\beta e_k}{2} + \log(\omega)\beta o_k\right)bo_k\right), \tag{17}$$

$$do = \sum_{k=0}^{n} e^{-\frac{\pi\beta o_k}{2}} \omega^{\beta e_k} \left(\sin\left(\frac{\pi\beta e_k}{2} + \log(\omega)\beta o_k \right) be_k + \cos\left(\frac{\pi\beta e_k}{2} + \log(\omega)\beta o_k \right) bo_k \right). \tag{18}$$

The frequency response of the plant can generally be written in terms of its gain and phase values as follows:

$$P(j\omega) = |P(j\omega)| e^{j\angle \mathrm{P}(j\omega)}. \tag{19}$$

As a result, Equation (20) gives the gain value of the plant frequency response.

$$|P(j\omega)| = K \sqrt{\frac{ne^2 + no^2}{de^2 + do^2}}. \tag{20}$$

Similarly, Equation (21) gives the phase value of the plant frequency response.

$$\angle \mathrm{P}(j\omega) = \arctan\left(\frac{no}{ne}\right) - \arctan\left(\frac{do}{de}\right) - L\omega. \tag{21}$$

As a consequence, the gain and phase equations for the universal plant's frequency response were found.

4 | DESIGN OF THE PID CONTROLLER

The PID controller's transfer function is described in Equation (22).

$$C(s) = k_p + \frac{k_i}{s} + k_d s. \tag{22}$$

As mentioned previously, the proportional coefficient is k_p, the integral coefficient is k_i, and the derivative coefficient is k_d. Equation (23) shows the frequency response of the PID controller.

$$C(j\omega) = k_p + \frac{k_i}{j\omega} + k_d(j\omega) = k_p - \frac{jk_i}{\omega} + jk_d\omega. \tag{23}$$

Shortly, the controller can be shown with its gain and phase values:

$$C(j\omega) = |C(j\omega)| e^{j\angle C(j\omega)}. \tag{24}$$

Equation (25) gives the gain value of the PID controller's frequency response.

$$|C(j\omega)| = \sqrt{k_p^2 + \left(-\frac{k_i}{\omega} + k_d\omega \right)^2}. \tag{25}$$

Equation (26) shows the phase value of the controller's frequency response.

$$\angle \mathrm{C}(j\omega) = \arctan\left(\frac{-\frac{\mathrm{k_i}}{\omega} + \mathrm{k_d}\omega}{\mathrm{k_p}}\right). \tag{26}$$

Thus, the frequency response of the PID controller is obtained.

5 | DESIGN OF THE AUTO TUNING SYSTEM

Using the frequency response of the plant and the controller, the following gives the frequency response of the system.

$$G(j\omega) = P(j\omega)C(j\omega). \tag{27}$$

The following equations provide a representation of the system's frequency response in terms of its constituent parts. It is evident that the system's gain might be computed by multiplying the gains of the controller and the plant independently. In a similar vein, the system phase might be produced by separately adding the plant and controller phases.

$$|G(j\omega)| = |P(j\omega)C(j\omega)| = |P(j\omega)||C(j\omega)|, \tag{28}$$

$$\angle \mathrm{G}(j\omega) = \angle \mathrm{P}(j\omega)\mathrm{C}(j\omega) = \angle \mathrm{P}(j\omega) + \angle \mathrm{C}(j\omega). \tag{29}$$

For simplicity, the following representations are employed at the gain crossover frequency with the aid of the previous notations.

$$\begin{matrix} gcne = ne|_{\omega=\omega_{gc}} & gcno = no|_{\omega=\omega_{gc}} \\ gcde = de|_{\omega=\omega_{gc}} & gcdo = do|_{\omega=\omega_{gc}} \end{matrix}. \tag{30}$$

Here, *gcne* is the abbreviation stands for the even part of the numerator polynomial at the gain crossover frequency. Similarly, *gcno* is the odd part of the numerator polynomial at ω_{gc}. The even and odd parts of the denominator polynomial are given in a similar way. Then, with the help of Equation (4), the gain of the system could be calculated with the following equation in brief.

$$\begin{aligned} \left|G\left(j\omega_{gc}\right)\right| &= \left|P\left(j\omega_{gc}\right)\right|\left|C\left(j\omega_{gc}\right)\right| \\ &= K\sqrt{\frac{gcne^2 + gcno^2}{gcde^2 + gcdo^2}}\sqrt{k_p^2 + \left(-\frac{k_i}{\omega_{gc}} + k_d\omega_{gc}\right)^2} = 1. \end{aligned} \tag{31}$$

Similarly, the phase of the system could be written in the following way according to Equation (3).

$$\begin{aligned} \angle \mathrm{G}\left(\mathrm{j}\omega_{gc}\right) &= \angle \mathrm{P}\left(\mathrm{j}\omega_{gc}\right) + \angle \mathrm{C}\left(\mathrm{j}\omega_{gc}\right) \\ &= \arctan\left(\frac{gcno}{gcne}\right) - \arctan\left(\frac{gcdo}{gcde}\right) - L\omega_{gc} + \arctan\left(\frac{-\frac{k_i}{\omega_{gc}} + k_d\omega_{gc}}{k_p}\right) = PM - \pi. \end{aligned} \tag{32}$$

Equation (32) is rewritten as Equation (33) to calculate the PID controller's performance coefficients.

$$\frac{-\frac{k_i}{\omega_{gc}} + k_d\omega_{gc}}{k_p} = \tan(\varphi_1). \tag{33}$$

The value of the φ_1 angle is defined in Equation (34).

$$\varphi_1 = PM - \pi - \arctan\left(\frac{gcno}{gcne}\right) + \arctan\left(\frac{gcdo}{gcde}\right) + L\omega_{gc}. \tag{34}$$

Thus far, the system's frequency characteristics at the gain crossover frequency have been determined. The last step involves calculating the PID controller's parameters by combining the answers for the system phase and gain equations. Here, $k_p = k_1$, $k_i = k_1 k_2$, and $k_d = k_1 k_3$ conversion is made in order to minimize the cost of calculation.

$$\begin{aligned} k_1 &= \pm \frac{\sqrt{gcde^2 + gcdo^2}}{K\sqrt{(gcne^2 + gcno^2)\sec(\varphi_1)^2}}, \\ k_2 &= \omega_{gc}\left(k_3\omega_{gc} - \tan(\varphi_1)\right). \end{aligned} \tag{35}$$

These controller parameters meet the system's gain and phase characteristics at the gain crossover frequency originally specified by Equations (3) and (4). Let's go over the process again for the phase crossover frequency's frequency requirements. For the even and odd parts of the numerator and the denominator polynomial at the phase crossover frequency, the following notations are provided.

$$\begin{aligned} pcne &= ne|_{\omega=\omega_{pc}} \quad pcno = no|_{\omega=\omega_{pc}} \\ pcde &= de|_{\omega=\omega_{pc}} \quad pcdo = do|_{\omega=\omega_{pc}} \end{aligned}. \tag{36}$$

The following formulations, which are similar to earlier equations, display the system's phase and gain, respectively, after taking into account Equations (5) and (6) at the phase crossover frequency.

$$\begin{aligned} &\left|G(j\omega_{pc})\right| = \left|P(j\omega_{pc})\right|\left|C(j\omega_{pc})\right| \\ &= K\sqrt{\frac{pcne^2 + pcno^2}{pcde^2 + pcdo^2}}\sqrt{k_p^2 + \left(-\frac{k_i}{\omega_{pc}} + k_d\omega_{pc}\right)^2} = 10^{GM/20} = DB, \end{aligned} \tag{37}$$

$$\begin{aligned} &\angle \mathrm{G}(j\omega_{pc}) = \angle \mathrm{P}(j\omega_{pc}) + \angle \mathrm{C}(j\omega_{pc}) \\ &= \arctan\left(\frac{pcno}{pcne}\right) - \arctan\left(\frac{pcdo}{pcde}\right) - L\omega_{pc} + \arctan\left(\frac{-\frac{k_i}{\omega_{pc}} + k_d\omega_{pc}}{k_p}\right) \\ &= -\pi. \end{aligned} \tag{38}$$

Similar to above, Equation (38) is rewritten as Equation (39) to calculate the PID controller's performance coefficients.

$$\frac{-\frac{k_i}{\omega_{pc}} + k_d\omega_{pc}}{k_p} = \tan(\varphi_2). \tag{39}$$

The value of φ_2 is defined in the following way.

$$\varphi_2 = -\pi - \arctan\left(\frac{pcno}{pcne}\right) + \arctan\left(\frac{pcdo}{pcde}\right) + L\omega_{pc}. \tag{40}$$

The controller settings for the intended frequency characteristics at the phase crossover frequency are provided by the combined solutions of the aforementioned equations. Again, $k_p = k_1$, $k_i = k_1 k_2$, and $k_d = k_1 k_3$ conversion is done to make the calculation easier.

$$k_1 = \pm \frac{DB\sqrt{pcde^2 + pcdo^2}}{K\sqrt{(pcne^2 + pcno^2)\sec(\varphi_2)^2}},$$
$$k_2 = \omega_{pc}\left(k_3\omega_{pc} - \tan(\varphi_2)\right). \tag{41}$$

Thus, the PID controller can be rewritten in the following form.

$$C(s) = k_p + \frac{k_i}{s} + k_d s = k_p\left(1 + \frac{1}{T_i s} + T_d s\right), \frac{T_i}{T_d} = 4. \tag{42}$$

Ziegler and Nichols introduced two traditional techniques for parameterizing PID controllers in 1942. These techniques are still frequently utilized, either unaltered or with slight adjustments [54]. According to Wallen et al. [55] the relationship between practical application and system performance was the primary factor in picking the ratio between T_i and T_d as 4. This link was presented using the modified Ziegler Nichols approach in numerous research published in the literature [3, 56, 57].

To meet the frequency requirements, two separate computations for both crossover frequencies are thus performed. Combining these two will result in a single controller that simultaneously meets the frequency criteria. Shortly, k_1 and k_2 in Equations (35) and (41) have to be combined separately. The DB and GM are derived by solving the k_1's in Equations (35) and (41) together. The phase crossover frequency and the gain crossover frequency are simultaneously obtained by solving all k_2 in these equations. This technique eliminates the requirement to supply an external number to the gain crossover frequency, allowing the device to operate at its maximum frequency range. The gain and phase crossover values of the aforementioned k_2 equations are determined by applying numerical analytical steps produced by tracing the common crossing points of the two equations to the gain crossover frequency. Consequently, the substitution strategy is used to obtain the k_p, k_i, and k_d values, and the specified unknowns are found. The replacement procedure is used to confirm the validity and accuracy of the data generated in the previous stage.

6 | CASE STUDY

In line with the plant structures of the system, three examples will be shown for complicated, fractional, and integer orders. The components of the most widely specified plant type and PID controller that have been suggested make up the system. As part of the stability study of the systems, bode diagrams, step responses, and responses to unforeseen load disturbances will be developed for each controlled system. In every application, the differences in the evolution of plant structure under continuous conditions—from the most basic to the most intricate—will be seen.

6.1 | Example 1: Integer order plant (IOP)

Let's think about the plant Equation (43) that Padulga and Visiolo [58] employed in their study.

$$P_1(s) = \frac{1}{s+1}e^{-0.1s}. \tag{43}$$

In this illustration, the PM is considered to be PM = 45°, and the target gain crossover frequency is $\omega_{gc} = 5rad/s$. As a result, Equation (44) illustrates the controller that may be found using Equations (35) and (41).

$$C_1(s) = 4.51621 + \frac{18.6657}{s} + 0.273177s. \tag{44}$$

Figure 3 shows the intersection point (A) and bode diagram (B) for the system, whose PM is assumed to be PM = 45°. Figure 3 reveals that the system that meets the required specifications may be easily generated by using the calculation formulae.

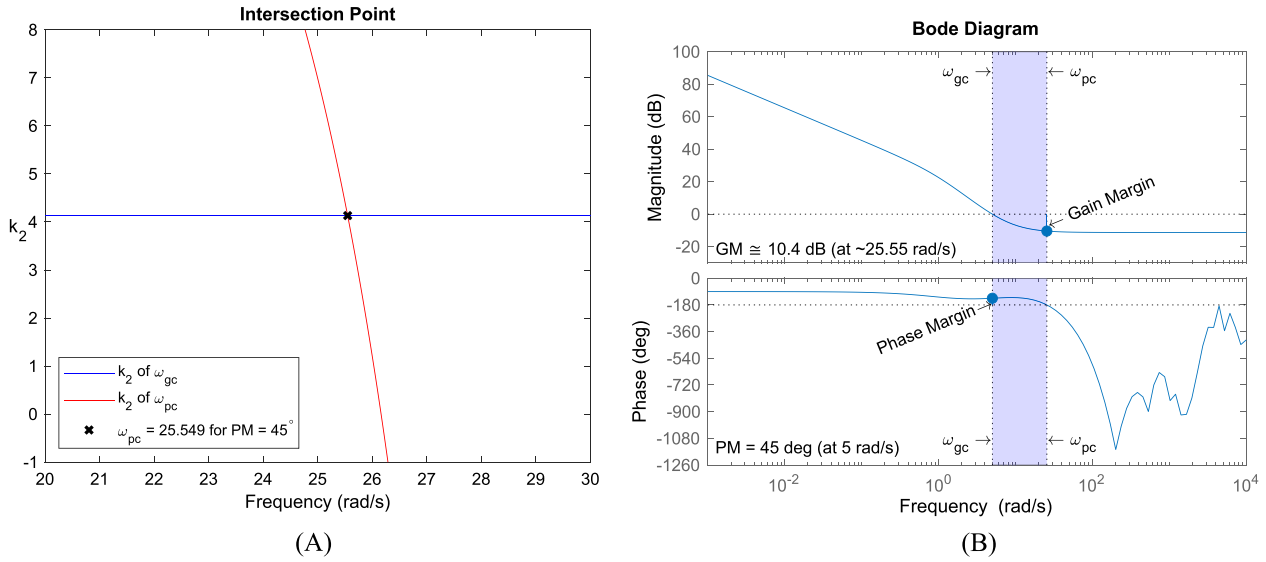

FIGURE 3 The system's (A) intersection point and (B) bode diagram with PM = 45°. [Colour figure can be viewed at wileyonlinelibrary.com]

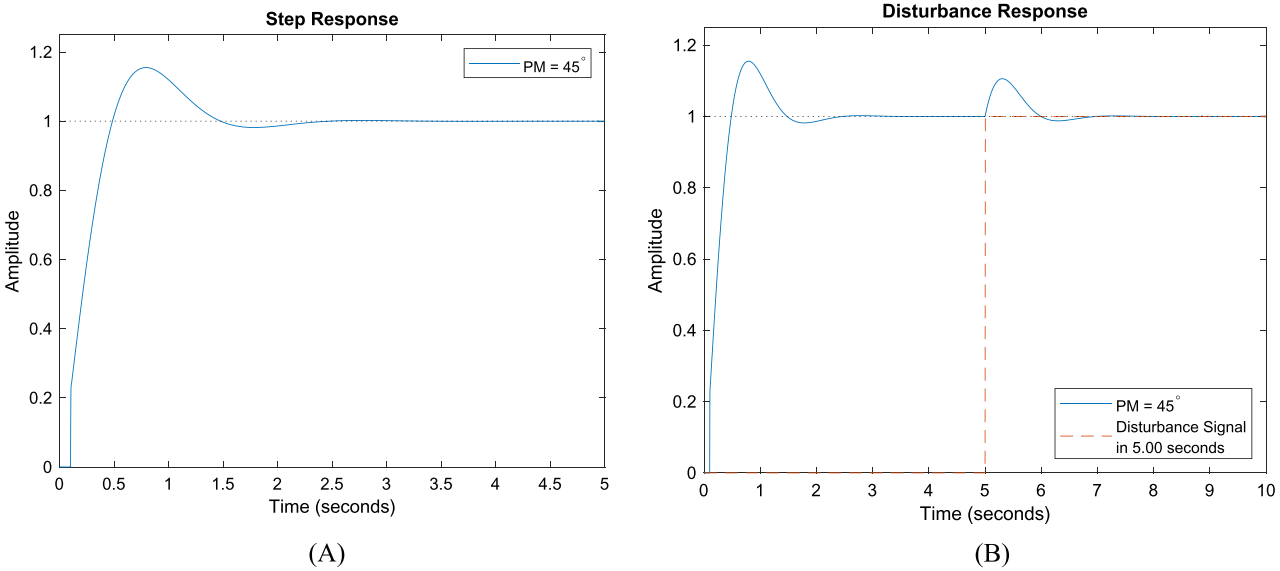

FIGURE 4 The system's (A) step response and (B) load disturbance reaction with PM = 45°. [Colour figure can be viewed at wileyonlinelibrary.com]

The system's step response (A) and response to a load disturbance (B) are displayed in Figure 4, where PM = 45° is the expected PM. It is clear that the system error reacts to unforeseen load disruptions at the lowest feasible level while exhibiting stability behavior in its step response.

Table 2 provides the phase crossover frequency, the GM, k_p, k_i, and k_d values for varying values of the PM w.r.t. $\omega_{gc} = 5\,\text{rad/s}$. The table's findings demonstrate that a rise in PM causes the phase crossover frequency to rise thus, the distance between ω_{gc} and ω_{pc} expands. This is where the PM's influence over the phase crossover frequency is visible.

Figure 5 shows the system's intersection points (A) and bode diagram (B), with the PM taken to be between [30°, 60°]. Here, the PM = 30° corresponds to the value of $\omega_{gc}{}^{<1>}$, whereas the PM = 60° corresponds to the value of the $\omega_{gc}{}^{<7>}$.

Figure 6 shows the step responses (A) and load disturbance responses (B) of the system with a PM between [30°, 60°]. The system's responsiveness to the unexpected load disturbance decreased below around 12% as a result.

TABLE 2 For PM variations, k_p, k_i, k_d, ω_{pc}, and GM values were discovered.

PM	ω_{gc}	ω_{pc}	GM	k_p	k_i	k_d
30°	5	22.4633	−13.70020	3.74963	21.3862	0.164355
35°	5	23.7377	−12.59390	4.03653	20.5363	0.198350
40°	5	24.7386	−11.48380	4.29270	19.6272	0.234717
45°	5	25.5489	−10.41300	4.51621	18.6657	0.273177
50°	5	26.2211	−9.39915	4.70534	17.6591	0.313439
55°	5	26.7899	−8.44823	4.85867	16.6152	0.355197
60°	5	27.2793	−7.56121	4.97501	15.5418	0.398132

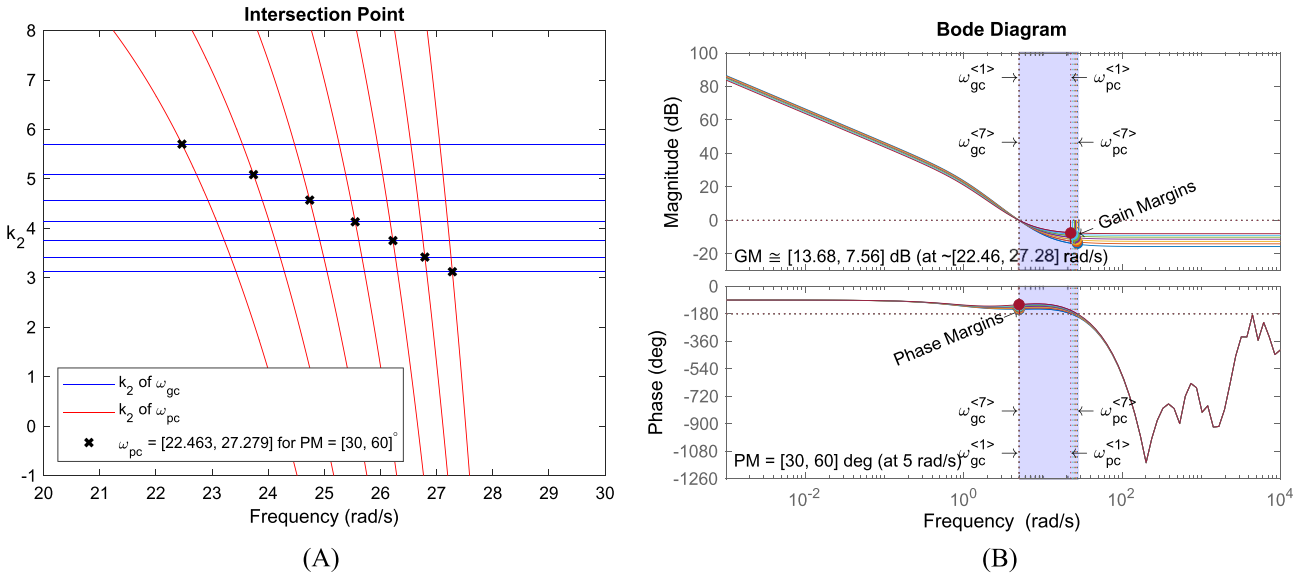

FIGURE 5 The system's (A) intersection points and (B) bode diagrams. [Colour figure can be viewed at wileyonlinelibrary.com]

The obtained bode diagrams, step responses, load disturbance responses, stability, and stability satisfactorily illustrate the system's calculation equations.

6.2 | Example 2: Fractional order plant (FOP)

Let's use the plant from Example 1 and convert the order value by 25% to obtain a fractional number.

$$P_2(s) = \frac{1}{s^{1.25}+1} e^{-0.1s}. \tag{45}$$

For this case, $\omega_{gc} = 5\,\text{rad/s}$ is once again taken into consideration as the ideal gain crossover frequency. Table 3 lists the performance coefficients of the controller k_p, k_i, and k_d obtained for desired frequency values. The PM is taken between 30° and 60° with a 5° of increment.

Once more, it is evident that increasing the PM results in a higher phase crossover frequency. It is evident how the fractionalized order affects the phase crossover frequency when comparing this plant to the one in the preceding example.

For every system in Table 3, the intersection points of the k_2 curves (A) and the Bode diagrams (B) are displayed in Figure 7. The necessary parameters are obviously satisfied.

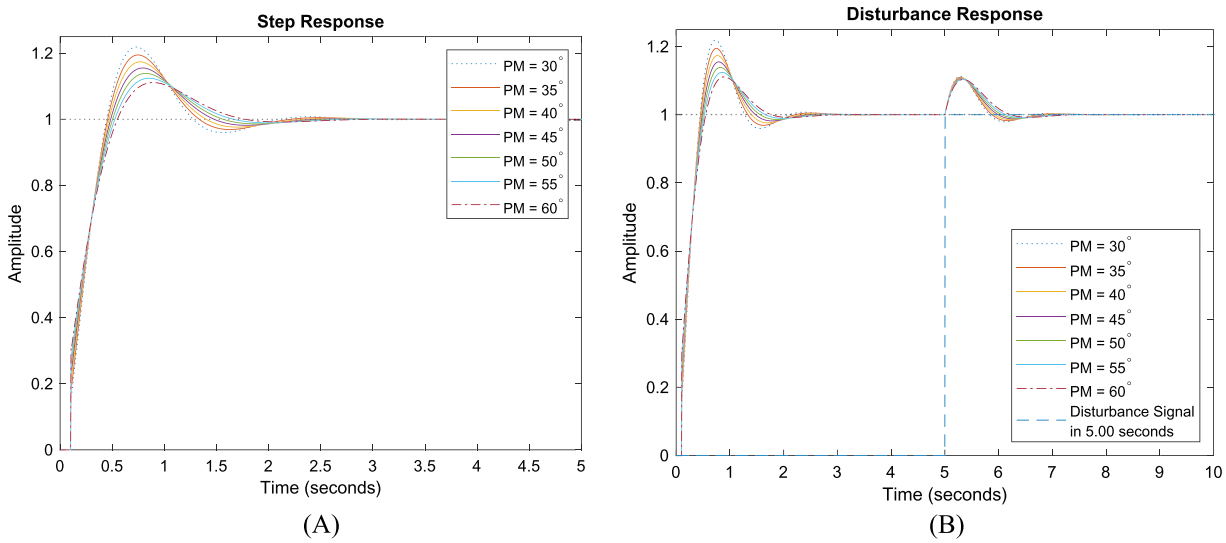

FIGURE 6 The system's (A) step responses and (B) load disturbance reactions. [Colour figure can be viewed at wileyonlinelibrary.com]

TABLE 3 For PM variations, k_p, k_i, k_d, ω_{pc}, and GM values were discovered.

PM	ω_{gc}	ω_{pc}	GM	k_p	k_i	k_d
30°	5	21.7335	−11.59960	6.86739	22.8963	0.514943
35°	5	22.3576	−10.85560	7.01597	21.3809	0.575559
40°	5	22.8936	−10.14620	7.11115	19.8389	0.637239
45°	5	23.3614	−9.47673	7.15220	18.2820	0.699514
50°	5	23.7751	−8.84948	7.13883	16.7221	0.761910
55°	5	24.1452	−8.26502	7.07113	15.1710	0.823952
60°	5	24.4796	−7.72298	6.94961	13.6406	0.885168

The initial step responses (A) and the ones under load disturbance (B) of the various systems listed in Table 3 are displayed in Figure 8. Consequently, at the time of the disruption, the system altered by less than 9% and recovered satisfactorily.

Therefore, on the plant with a fractional order, the suggested technique effectively attained system resilience and stability.

In this example, the order of the plant is modified to have a complex part with its conjugate.

$$P_{3,4}(s) = \frac{1}{s^{1.25\mathrm{mj}0.25} + 1} \mathrm{e}^{-0.1s}. \tag{46}$$

There are two different forms of this plant. Both the first and the second have complicated orders with positive and negative imaginary parts, respectively. The target gain crossover frequency is once more $\omega_{gc} = 5\,\mathrm{rad/s}$. For the plant with a negative imaginary component, Table 4 displays the unknown parameters for varying PM values at $\omega_{gc} = 5\,\mathrm{rad/s}$.

In the same way, Table 5 displays the plant's unknown characteristics for the positive imaginary component.

The phase crossover frequency may be expressed as increasing with the PM. The GM falls when there is a negative imaginary component and rises when there is a positive imaginary component.

The Bode diagrams for systems with negative imaginary parts, whose PM is between PM = [30°, 60°] degrees, are displayed in Figure 9A. Additionally, the Bode diagrams for the systems with positive imaginary parts are displayed in Figure 9B.

The intersection locations of k_2 curves for systems having a negative imaginary component are displayed in Figure 10A, while those for systems with a positive imaginary part are displayed in Figure 10B.

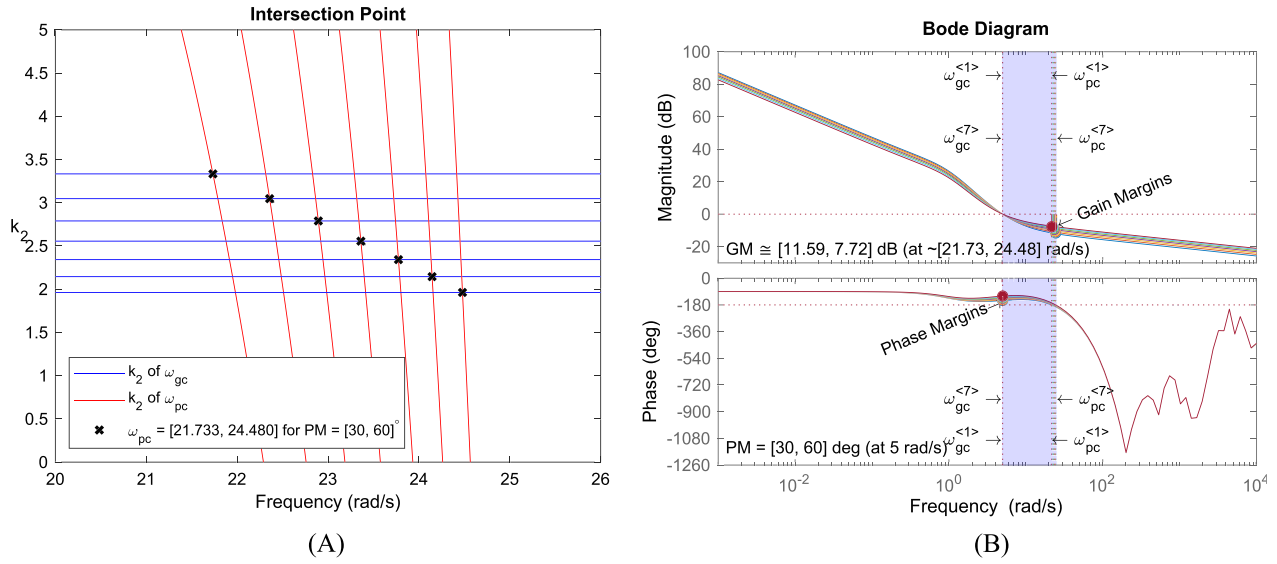

FIGURE 7 The system's (A) intersection points and (B) bode diagrams. [Colour figure can be viewed at wileyonlinelibrary.com]

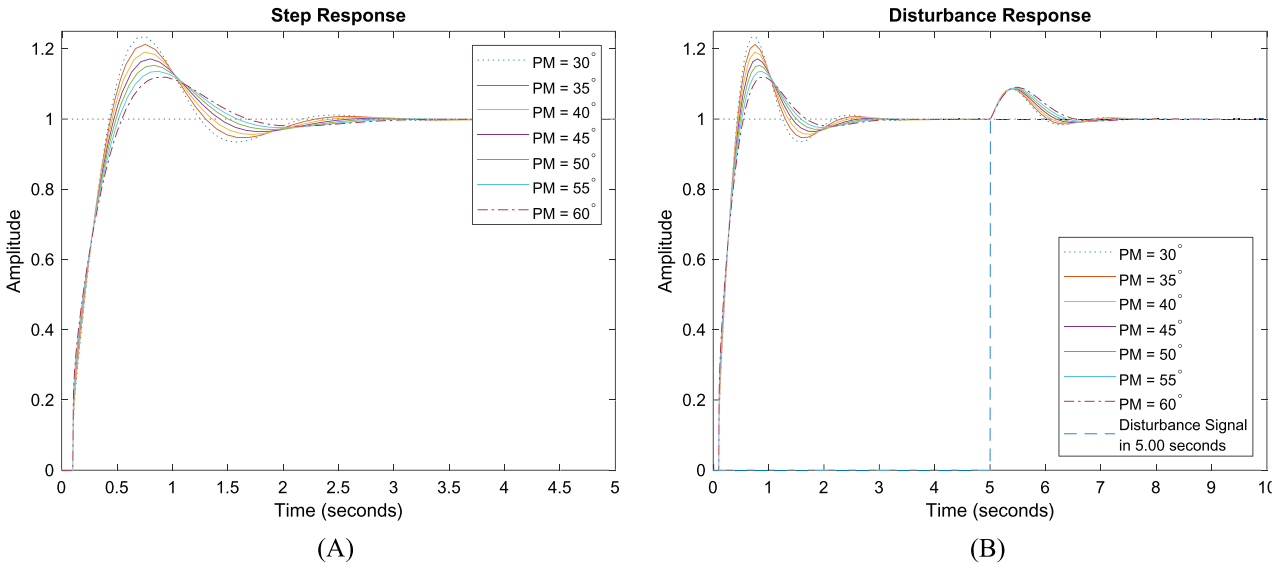

FIGURE 8 The system's (A) step responses and (B) load disturbance reactions. [Colour figure can be viewed at wileyonlinelibrary.com]

Consequently, the method's impact on the FCOP is demonstrated. The results are discussed in some detail in the next section.

7 | DISCUSSION

The research examines a sophisticated plant model incorporating integer, fractional, and complex coefficients, as well as exponential and time-delayed terms. This model is analyzed within a suggested framework and is expected to be effectively controlled using a traditional PID controller. The study highlights the connection between the closed-loop and open-loop transfer functions, using Bode diagrams to assess the latter. To mitigate the impact of unexpected load disturbances, the design approach is particularly important. Additionally, simulations are crucial to minimize costs associated with potential inaccuracies. The paper initially focuses on the IOP. To address overshoot issues caused by unexpected load disturbances, the exponential value is adjusted to 25% to create a FOP. This paper then transitions to the FCOP by converting the virtual exponential value of 25% into a complex exponential.

TABLE 4 For PM changes relative to the negative imaginary component, k_p, k_i, k_d, ω_{pc}, and GM values were discovered.

PM	ω_{gc}	ω_{pc}	GM	k_p	k_i	k_d
30°	5	29.4660	−16.92980	8.87967	44.5844	0.442131
35°	5	30.3105	−15.76230	9.43037	42.5858	0.522074
40°	5	31.0037	−14.66440	9.90929	40.4748	0.606513
45°	5	31.5851	−13.64010	10.31280	38.2676	0.694804
50°	5	32.0817	−12.68820	10.63780	35.9807	0.786277
55°	5	32.5124	−11.80570	10.88190	33.6318	0.880234
60°	5	32.8907	−10.98900	11.04310	31.2387	0.975961

TABLE 5 For PM changes relative to the positive imaginary component, k_p, k_i, k_d, ω_{pc}, and GM values were discovered.

PM	ω_{gc}	ω_{pc}	GM	k_p	k_i	k_d
30°	5	15.0538	−7.74174	4.37395	10.0156	0.477540
35°	5	15.6042	−7.33345	4.32379	9.0663	0.515516
40°	5	16.0862	−6.92938	4.24072	8.1314	0.552909
45°	5	16.5148	−6.53993	4.12538	7.2182	0.589436
50°	5	16.9005	−6.17129	3.97864	6.3337	0.624819
55°	5	17.2516	−5.82719	3.80162	5.4844	0.658788
60°	5	17.5739	−5.50991	3.59567	4.6770	0.691086

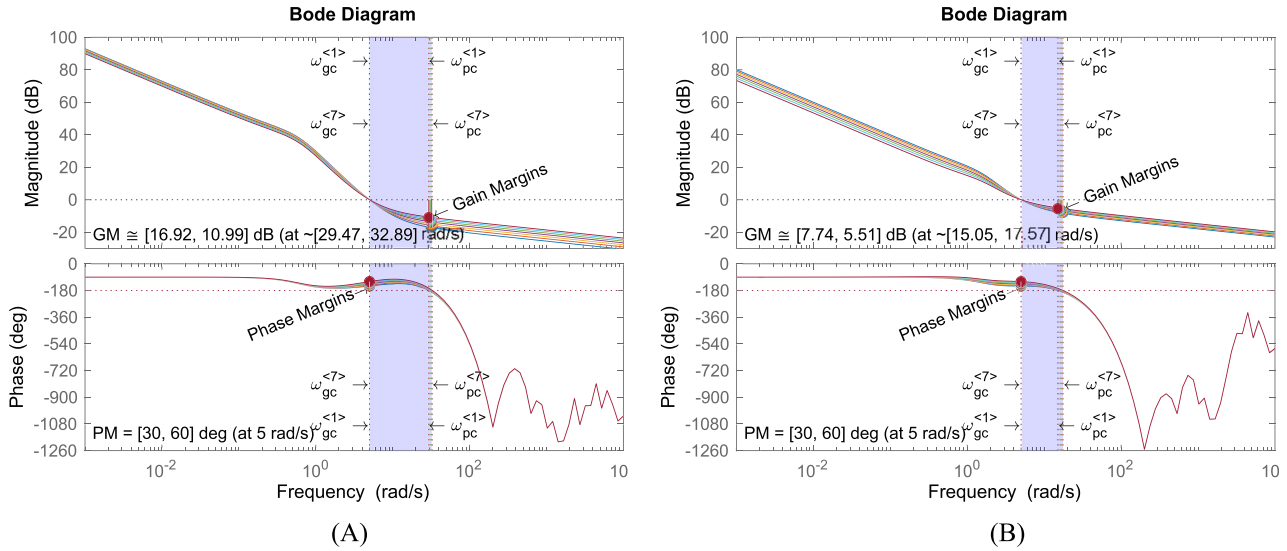

(A) (B)

FIGURE 9 The bode diagrams (A) for systems having negative imaginary part, (B) for systems having positive imaginary part. [Colour figure can be viewed at wileyonlinelibrary.com]

Step response and load disturbance response examples for the system with a PM of 45° are shown in Figure 11A,B, respectively. The step responses of the FOP and IOP are similar. However, the FOP demonstrated improvements in settling time and overshoot time. Additionally, the fractionalized plant exhibited fewer system failures and a faster response to unexpected load disturbances compared to the integer plant.

For these cases, the system's bode diagram is displayed in Figure 12: (A) close view and (B) distant view.

The points labeled 1 and 2 in Examples 1 and 2 represent the gain crossover and phase crossover frequencies, respectively. In Example 3, these frequencies are shown as points 3 and 4 for the positive and negative imaginary parts of the system. The left points represent the gain crossover frequency, while the right points indicate the phase crossover

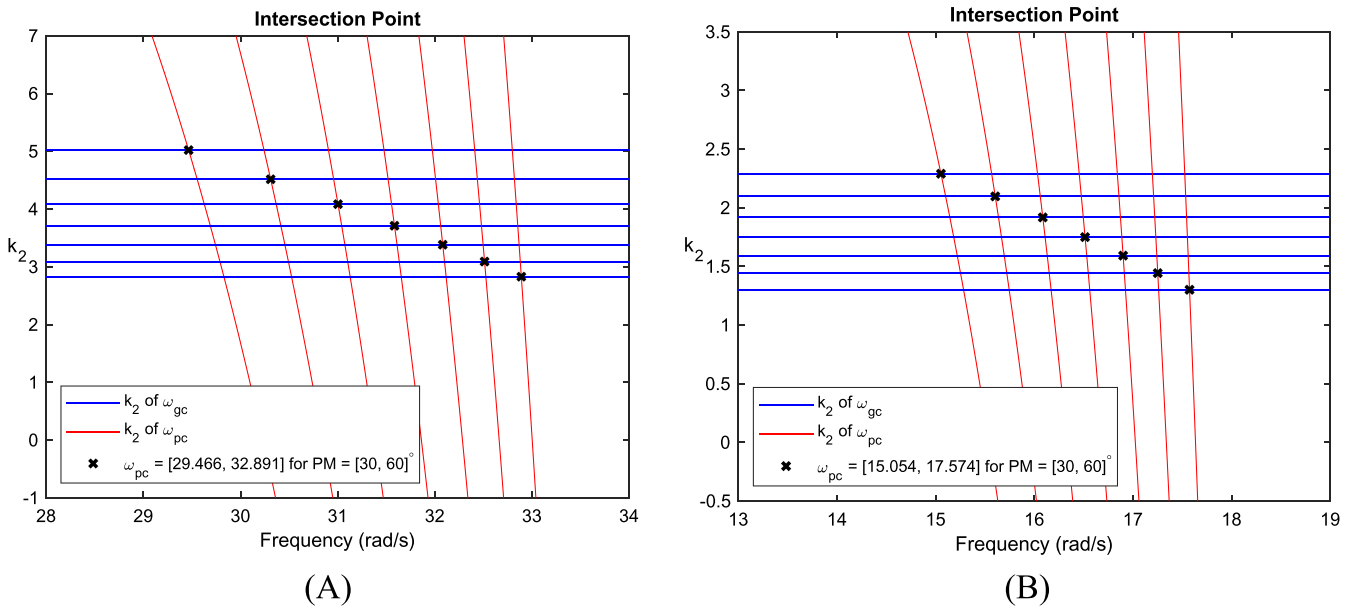

FIGURE 10 The intersection points (A) for systems having negative imaginary part, (B) for systems having positive imaginary part. [Colour figure can be viewed at wileyonlinelibrary.com]

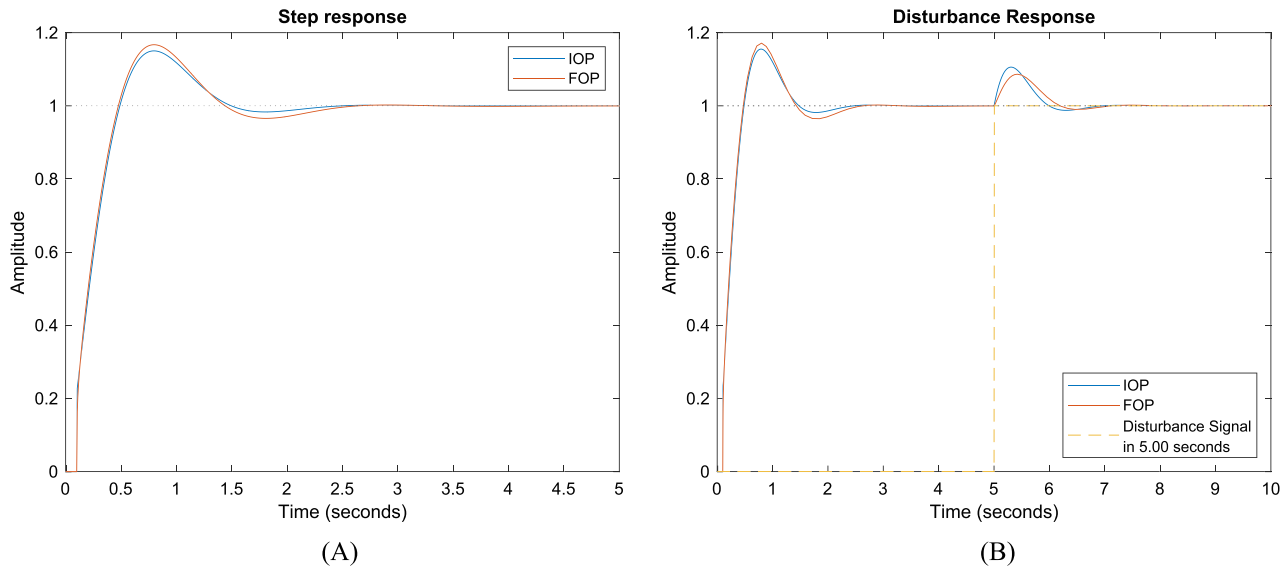

FIGURE 11 The systems' (A) step response and (B) load disturbance reaction with PM = 45°. [Colour figure can be viewed at wileyonlinelibrary.com]

frequency. This visual representation demonstrates how the plant's order change influences the phase crossover frequency. If the ω_{pc} of the IOP labeled with 1 is centered, the ω_{pc} of the FOP moved left. Besides, the complex order plant with negative conjugate caused the ω_{pc} to move right, and the one with positive conjugate caused the ω_{pc} to move left. The changes in crossover frequencies between fractional and IOPs are important to consider when modifying the plant order. Ensuring a wide stability margin is crucial. FOPs reduce the separation between the two crossover frequencies compared to IOPs, while complex order plants with negative imaginary components increase this distance. Despite the apparent shift in PM, the GM remains relatively unaffected, supporting the complex number theory. This suggests that the imaginary component of the complex order plant influences more than just the phase crossover frequency location.

It would be beneficial to discuss about the difficulties and assumptions faced throughout the design process. The design is based on satisfying gain and phase crossover frequencies towards the researcher's desire. Two different controllers were tuned for this purpose. The first one satisfies the desired gain crossover frequency. The second one is for

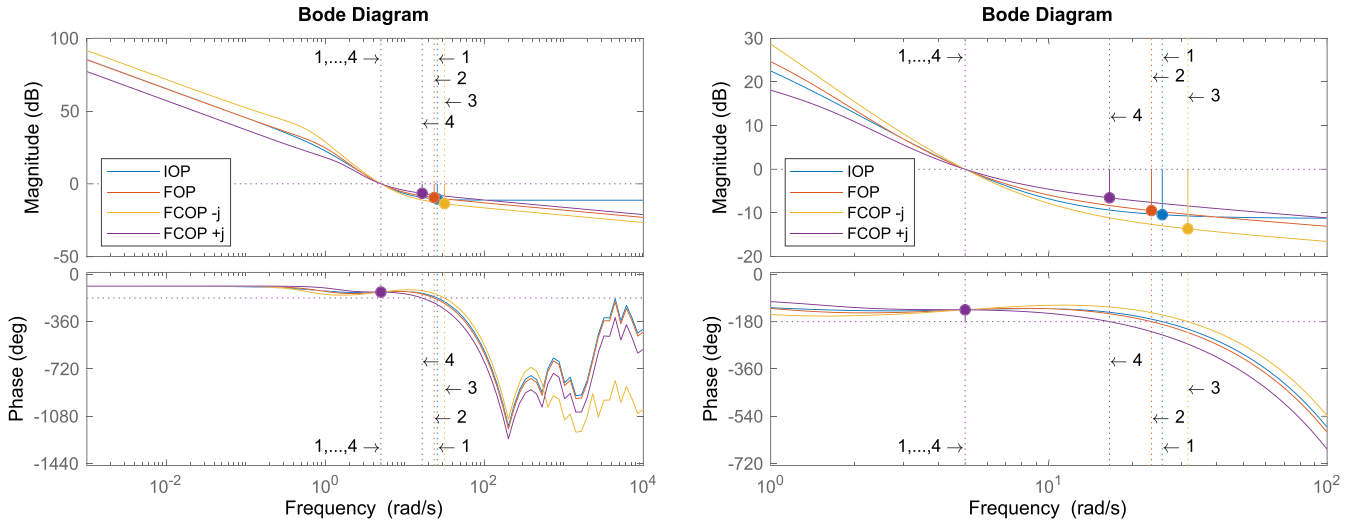

FIGURE 12 The bode diagrams with PM = 45° (A) for systems having negative imaginary part, (B) for systems having positive imaginary part. [Colour figure can be viewed at wileyonlinelibrary.com]

the phase crossover frequency. At the final stage, these two controllers were combined to satisfy these two specifications at the same time. There presented two specifications for the gain crossover frequency (Equation 3 and Equation 4). Since there are three parameters in PID controller structure, it became challenging to find three unknown variables using two equations. To overcome this, an assumption of $k_p = k_1$, $k_i = k_1 k_2$, and $k_d = k_1 k_3$ is done. This can be found in the paragraphs before Equations (35) and (41). With the help of this conversion, the parameters of the PID controller were successfully obtained.

8 | CONCLUSION

This study focuses on the analysis of physical changes in the plant model with the most general structure, which is named as the FCOP. This model is built to cover plants having integer, real, and/or complex number coefficients and/or orders. Thus, by properly changing the coefficients and orders, three different types of plants can easily be obtained. Moreover, time delay can also be added. The aim is to provide stability and robustness to the system with the help of a controller. To achieve this purpose, the classical proportional integral derivative controller was used. By correctly tuning the controller consisting of three parameters, it was aimed to provide the desired stability and robustness of the system. There are different methods proposed in the literature to achieve stability and robustness. One of the most effective methods is flattening the phase curve in the system frequency response within a certain range. In many studies, the flattening process is achieved by taking the derivative of the system phase curve at a point called the tangent frequency and equating it to zero. This method is effective, but it causes complex mathematical equations to become even more complicated and therefore increases the computational cost. The method in this paper brings a graphical perspective to the flattening process of the phase curve. The phase curve will be flattened in the region between the gain crossover frequency and the phase crossover frequency. By appropriately tuning these two crossover frequency values, the phase curve will also be relatively flattened. This can be thought of as flattening a rope pulled from both ends. If the two ends of the rope represent two crossover frequencies, these crossover frequencies can be extended outward and the curve in between can be flattened. The most important advantage of the method can be said to be that it provides reliable formulas without causing mathematical complexity. Also, the crossover frequencies can easily be tuned towards researcher's desire. The most important disadvantage is that the correct operation of the method depends on the selection of the suitable frequencies in a way that will ensure system stability. Although the method is effective, robustness will not be achieved in a system that has not reached stability. By this study, the effect of an integer order controller on various plants has been shown. For future studies, the study can be modified and optimized for more different types of models.

AUTHOR CONTRIBUTIONS

Uğur Demiroğlu: Methodology; validation; visualization. **Bilal Şenol:** Supervision; writing—original draft; writing—review and editing; formal analysis. **Radek Matušů:** Validation; supervision; formal analysis; writing—original draft.

REFERENCES

1. R. Villafuerte-Segura, B. A. Itzá-Ortiz, P. A. López-Pérez, and E. Alvarado-Santos, *Mathematical model with time-delay and delayed controller for a bioreactor*, Math. Meth. Appl. Sci. **46** (2023), no. 1, 248–266.
2. C. I. Muresan and R. de Keyser, *Revisiting Ziegler-Nichols. A fractional order approach*, ISA Trans. **129** (2022), 287–296.
3. Y. Chen, C. Hu, and K. L. Moore, *Relay feedback tuning of robust PID controllers with iso-damping property*, In *42nd IEEE international conference on decision and control (IEEE Cat. No. 03CH37475)*, IEEE, 2003.
4. K. J. Åström and T. Hägglund, *Revisiting the Ziegler–Nichols step response method for PID control*, J. Process Control **14** (2004), no. 6, 635–650.
5. A. A. Jamil, W. F. Tu, S. W. Ali, Y. Terriche, and J. M. Guerrero, *Fractional-order PID controllers for temperature control: a review*, Energies **15** (2022), no. 10, 1–28.
6. A. Kochubei and Y. Luchko, *Fractional differential equations*, Walter de Gruyter GmbH & Co KG, 2019.
7. C. A. Monje, Y. Q. Chen, B. M. Vinagre, D. Xue, and V. Feliu, *Fractional-order systems and controls: fundamentals and applications*, Springer Science & Business Media, 2010.
8. Y. Q. Chen and K. L. Moore, *Discretization schemes for fractional-order differentiators and integrators*, IEEE Trans. Circuits Syst. I **49** (2002), no. 3, 363–367.
9. Ü. Lepik and H. Hein, *Fractional calculus*, In *Haar wavelets*, Springer, 2014, 107–122.
10. J. G. Ziegler and N. B. Nichols, *Optimum settings for automatic controllers*, ASME Trans. **64** (1942), no. 8, 759–765.
11. X. Li and L. Gao, *A simple frequency-domain tuning method of fractional-order PID controllers for fractional-order delay systems*, Int. J. Control Autom. Syst. **20** (2022), 1–10.
12. A. Maachou, R. Malti, P. Melchior, J. L. Battaglia, and B. Hay, *Thermal system identification using fractional models for high temperature levels around different operating points*, Nonlinear Dyn. **70** (2012), no. 2, 941–950.
13. S. Luo, F. L. Lewis, Y. Song, and K. G. Vamvoudakis, *Adaptive backstepping optimal control of a fractional-order chaotic magnetic-field electromechanical transducer*, Nonlinear Dyn. **100** (2020), no. 1, 523–540.
14. E. Loghman, A. Kamali, F. Bakhtiari-Nejad, and M. Abbaszadeh, *Nonlinear free and forced vibrations of fractional modeled viscoelastic FGM micro-beam*, App. Math. Model. **92** (2021), 297–314.
15. J. Shi, J. Zheng, X. Liu, W. Xiang, and Q. Zhang, *Novel short-time fractional Fourier transform: theory, implementation, and applications*, IEEE Trans. Signal Process **68** (2020), 3280–3295.
16. Y. Wang, H. Zhong, and B. Wang, *Fractional order model of three-winding series-connected single-phase motor*, In *2017 20th international conference on electrical machines and systems (ICEMS)*, IEEE, 2017.
17. P. Liu, Z. Zeng, and J. Wang, *Asymptotic and finite-time cluster synchronization of coupled fractional-order neural networks with time delay*, IEEE Trans. Neural Netw. Learn. Syst. **31** (2020), no. 11, 4956–4967.
18. P. Chen, B. Wang, Y. Tian, and Y. Yang, *Finite-time stability of a time-delay fractional-order hydraulic turbine regulating system*, IEEE Access **7** (2019), 82613–82623.
19. L. Bai and D. Xue, *Universal block diagram based modeling and simulation schemes for fractional-order control systems*, ISA Trans. **82** (2018), 153–162.
20. D. Li, L. Wei, T. Song, and Q. Jin, *Study on asymptotic stability of fractional singular systems with time delay*, Int. J. Control Autom. Syst. **18** (2020), no. 4, 1002–1011.
21. D. Li, X. He, T. Song, and Q. Jin, *Fractional order IMC controller design for two-input-two-output fractional order system*, Int. J. Control Autom. Syst. **17** (2019), no. 4, 936–947.
22. V. Feliu-Batlle, R. Rivas-Perez, and F. J. Castillo-García, *Simple fractional order controller combined with a Smith predictor for temperature control in a steel slab reheating furnace*, Int. J. Control Autom. Syst. **11** (2013), no. 3, 533–544.
23. V. V. Patel, *Ziegler–Nichols tuning method: understanding the PID controller*, Resonance **25** (2020), no. 10, 1385–1397.
24. S. Tufenkci, B. Senol, B. B. Alagoz, and R. Matušů, *Disturbance rejection FOPID controller design in v-domain*, J. Adv. Res. **25** (2020), 171–180.
25. I. Podlubny, *Fractional differential equations*, Academic Press, San Diego, CA, 1999.
26. S. Patnaik, J. P. Hollkamp, and F. Semperlotti, *Applications of variable-order fractional operators: a review*, Proc. R Soc. A. **476** (2020), no. 2234, 1–32.
27. U. Saeed, *A method for solving Caputo–Hadamard fractional initial and boundary value problems*, Math. Meth. Appl. Sci. **46** (2023), no. 13, 13907–13921.
28. H. Duy Binh, N. Dinh Huy, A. Tuan Nguyen, and N. Huu Can, *On nonlinear Sobolev equation with the Caputo fractional operator and exponential nonlinearity*, Math. Meth. Appl. Sci. **47** (2024), no. 3, 1492–1513.
29. S. Das, S. Saha, S. Das, and A. Gupta, *On the selection of tuning methodology of FOPID controllers for the control of higher order processes*, ISA Trans. **50** (2011), no. 3, 376–388.
30. C. A. Monje, A. J. Calderon, B. M. Vinagre, and Y. Q. Chen, *On fractional PIλ controllers: some tuning rules for robustness to plant uncertainties*, Nonlinear Dyn. **38** (2004), no. 1, 369–381.

31. G. Maione and P. Lino, *New tuning rules for fractional PIα controllers*, Nonlinear Dyn. **49** (2007), no. 1, 251–257.
32. M. Shahiri, A. Ranjbar, M. R. Karami, and R. Ghaderi, *New tuning design schemes of fractional complex-order PI controller*, Nonlinear Dyn. **84** (2016), no. 3, 1813–1835.
33. M. G. Moghadam, F. Padula, and L. Ntogramatzidis, *Tuning and performance assessment of complex fractional-order PI controllers*, IFAC-PapersOnLine **51** (2018), no. 4, 757–762.
34. C. I. Muresan, E. H. Dulf, and R. Both, *Vector-based tuning and experimental validation of fractional-order PI/PD controllers*, Nonlinear Dyn. **84** (2016), no. 1, 179–188.
35. A. Guefrachi, S. Najar, M. Amairi, and M. Aoun, *Tuning of a PI x+ iy D Fractional complex order controller*, In *25th Mediterranean conference on control and automation (MED)*, IEEE, 2017.
36. O. Hanif, G. B. Babu, and S. Sharma, *Performance improvement of PI x+ iy D fractional complex order controller using genetic algorithm*, In *Fourth international conference on advances in electrical, electronics, information, communication and bio-informatics (AEEICB)*, IEEE, 2018.
37. A. Bueno-Orovio and K. Burrage, *Complex-order fractional diffusion in reaction-diffusion systems*, Commun. Nonlinear Sci. **119** (2023), 107120.
38. A. Elwakil, C. Psychalinos, B. Maundy, and A. Allagui, *On the possible realization of a complex-order capacitive impedance and its applications*, Int. J. Circ. Theor. App. **51** (2023), no. 1, 500–507.
39. M. Zheng, G. Zhang, and T. Huang, *Tuning of fractional complex-order direct current motor controller using frequency domain analysis*, Math. Meth. Appl. Sci. **44** (2021), no. 4, 3167–3181.
40. R. Sekhar, T. P. Singh, and P. Shah, *Complex order PI α D γ design for surface roughness control in machining CNT Al-Mg hybrid composites*, Adv. Sci. Technol. Eng. Syst. J. **5** (2020), 299–306.
41. A. V. Tare, J. A. Jacob, V. A. Vyawahare, and V. N. Pande, *Design of novel optimal complex-order controllers for systems with fractional-order dynamics*, Int. J. Dynam. Control **7** (2019), no. 1, 355–367.
42. O. Saleem, F. Abbas, and J. Iqbal, *Complex fractional-order LQIR for inverted pendulum-type robotic mechanisms: design and experimental validation*, Mathematics **11** (2023), no. 4, 913.
43. A. Pratap, R. Raja, J. Cao, C. Huang, M. Niezabitowski, and O. Bagdasar, *Stability of discrete-time fractional-order time-delayed neural networks in complex field*, Math. Meth. Appl. Sci. **44** (2021), no. 1, 419–440.
44. U. Demiroğlu, B. Şenol, and R. Matušů, *An examination of complex fractional order physical phenomena in IOPD controller design*, Math. Meth. Appl. Sci. **46** (2023), no. 14, 15073–15093.
45. B. C. Kuo and M. F. Golnaraghi, *Automatic control systems*, Vol. **8**, Prentice hall, Englewood Cliffs, NJ, 1995.
46. B. Şenol and U. Demiroğlu, *Fractional order proportional derivative control for first order plus time delay plants: achieving phase and gain specifications simultaneously*, Trans. Inst. Meas. Control **41** (2019), no. 15, 4358–4369.
47. B. Şenol, U. Demiroğlu, and R. Matušů, *Fractional order proportional derivative control for time delay plant of the second order: the frequency frame*, J. Franklin Inst. **357** (2020), no. 12, 7944–7961.
48. B. Şenol and U. Demiroğlu, *Frequency frame approach on loop shaping of first order plus time delay systems using fractional order PI controller*, ISA Trans. **86** (2019), 192–200.
49. U. Demiroğlu and B. Şenol, *Frequency frame approach on tuning FOPI controller for TOPTD thermal processes*, ISA Trans. **108** (2021), 96–105.
50. M. Moradi and S. Seyedtabaii, *Intelligent fuzzy controller design: Disturbance rejection case*, Appl. Soft Comput. **124** (2022), 109015.
51. K. Hu and W. Zhang, *Position control algorithm of fuzzy adaptive PID of hydraulic interconnected suspension under load impact disturbance*, IEEE Access **10** (2022), 39665–39673.
52. F. Fayaz and G. Lal Pahuja, *Disturbance rejection based fractional order PID controller for system performance improvement of hybrid power system*, Optim. Control Appl. Meth. **43** (2022), no. 6, 1688–1706.
53. A. N. Karanam and B. Shaw, *A new two-degree of freedom combined PID controller for automatic generation control of a wind integrated interconnected power system*, Prot. Control Mod. Power Syst. **7** (2022), no. 1, 1–16.
54. K. J. Åström and T. Hägglund, *PID controllers: theory, design, and tuning*, ISA, Research Triangle Park, NC, USA, 1995.
55. A. Wallén, K. J. Åström, and T. Hägglund, *Loop-shaping design of PID controllers with constant Ti/Td RATIO*, Asian J. Control **4** (2002), no. 4, 403–409.
56. Y. Q. Chen, K. L. Moore, B. M. Vinagre, and I. Podlubny, *Robust PID controller autotuning with an Iso-damping property through a phase shaper*, In *Proceedings of the international conference on fractional differentiation and its applications*, Springer, 2005.
57. C. C. Hang, K. J. Åström, and W. K. Ho, *Refinements of the Ziegler–Nichols tuning formula*, In *IEEE proceedings D (control theory and applications)*, IEEE, 1991.
58. F. Padula and A. Visioli, *Tuning rules for optimal PID and fractional-order PID controllers*, J. Process Control **21** (2011), no. 1, 69–81.

How to cite this article: U. Demiroğlu, B. Şenol, and R. Matušů, *Analytical approach in designing PID controller for complex fractional order transfer function*, Math. Meth. Appl. Sci. (2024), 1–19, DOI 10.1002/mma.10579.